Wood Gas Processing To Generate Pure Hydrogen Suitable for PEM Fuel Cells

ARTICLE *in* ACS SUSTAINABLE CHEMISTRY & ENGINEERING · DECEMBER 2014

Impact Factor: 4.64 · DOI: 10.1021/sc500436m

ACS Sustainable Chemistry & Engineering

Research Article

pubs.acs.org/journal/ascecg

Wood Gas Processing To Generate Pure Hydrogen Suitable for PEM Fuel Cells

Silvester Fail,*[,†] Nicolas Diaz,*[,†,‡] Florian Benedikt,[†] Michael Kraussler,[†] Julian Hinteregger,[†] Klaus Bosch,[§] Marius Hackel,[∥] Reinhard Rauch,[†,‡] and Hermann Hofbauer[†,‡]

[†]Vienna University of Technology, Institute of Chemical Engineering, Getreidemarkt 9/166, Vienna 1060, Austria

[‡]Bioenergy 2020+ GmbH, Inffeldgasse 21b, Graz 8010, Austria

[§]Energie Burgenland AG, Kasernenstrasse 9, Eisenstadt 7000, Austria

[∥]Frankfurt Research and Technology Center (FRTC), Air Liquide, Forschung und Entwicklung GmbH, Gwinnerstrasse 27−33 , Frankfurt 60388, Germany

Supporting Information

ABSTRACT: A test campaign was carried out to generate renewable hydrogen based on wood gas derived from the commercial biomass steam gasification plant in Oberwart, Austria. The implemented process consisted of four operation units: (I) catalyzed water−gas shift (WGS) reaction, (II) gas drying and cleaning in a wet scrubber, (III) hydrogen purification by pressure swing adsorption, and (IV) use of the generated biohydrogen ($BioH_2$) in a proton exchange membrane (PEM) fuel cell. For almost 250 h, a reliable and continuous operation was achieved. A total of 560 ($L_{n\ dry\ basis\ (db)}$)/h of wood gas were extracted to produce 280 ($L_{n\ db}$)/h of $BioH_2$ with a purity of 99.97 vol $\%_{db}$. The catalyzed WGS reaction enabled a hydrogen recovery of 128% $(\dot{n}_{BioH_2})/(\dot{n}_{H_2,wood\ gas})$ over the whole process chain. An extensive chemical analysis of the main gas components and trace components (sulfur, C_xH_y, and ammonia) was carried out. No PEM fuel cell poisons were measured in the generated $BioH_2$. The only detectable impurities in the product were 0.02 vol $\%_{db}$ of O_2 and 0.01 vol $\%_{db}$ of N_2.

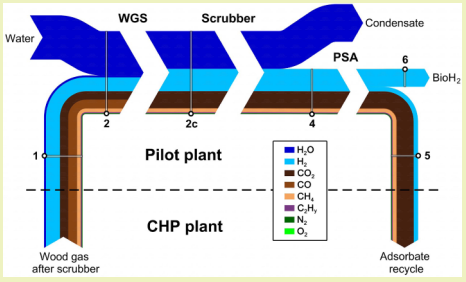

KEYWORDS: *Biohydrogen, Biomass, Gasification, Product gas, Water−gas shift, Gas scrubbing, Pressure swing adsorption, Latex*

INTRODUCTION

Hydrogen is required chiefly for the synthesis of ammonia and methanol as well as for various applications in refineries. In 2007, the world's installed capacity of production was about 65 million tons of hydrogen.[1] Its demand is growing especially because of the usage of heavier and dirtier feedstock in refineries that requires greater amounts of hydrogen for hydrotreating and hydrocracking.[2] Some authors consider a global hydrogen economy as the future perspective to cover the demands for electricity, heat, and transportation.[3,4] This would require a further increase in the production capacity. A total of 96% of the current hydrogen production is directly based on fossil fuels, mainly natural gas (49%).[1]

Considerable research has been carried out in the field of renewable hydrogen production. It can be distinguished between thermochemical, electrochemical, and biological approaches.[5] Especially, the increasing number of power-to-gas concepts, which use the excess electricity from wind power and photovoltaics for the hydrogen production in electrolyzers, should be pointed out.[6] This article deals with hydrogen production via the thermochemical processing of biomass, which is reported to be more costly than the conventional production methods but competitive with the electrolysis of water using renewable electricity.[7,8] Life cycle assessment of gasification-derived biohydrogen shows reduced greenhouse gas emissions compared to steam reforming of natural gas and a low nonrenewable energy demand.[9,10]

The established process chain for biohydrogen ($BioH_2$, here defined as hydrogen generated by or out of biomass) production was operated with a partial flow of wood gas (also product gas, producer gas, syngas, or synthesis gas) derived from the commercial biomass gasification plant in Oberwart, Austria. A total of 8.7 MW of wood chip power (23,000 (t_{wood})/a) is converted to 2.5 MW of electrical power and 3.5 MW of district heat.[11] The flowchart of the gasification power plant Oberwart is illustrated in Figure 1.

The design of this combined heat and power (CHP) plant is based on the well-documented plant in Güssing, Austria.[13] Both plants employ the dual fluidized bed (DFB) steam gasification technology. Wood gas is generated, cooled, filtered, cleaned, and finally burned in gas engines to generate electricity and district heat. Unlike the plant in Güssing, a biomass dryer and an organic rankine cycle (ORC) are employed in the CHP plant Oberwart.[14] The investigated pilot plant for hydrogen production was operated with a partial flow of wood gas extracted after its gas cleaning units. Therefore, particles were

Received: July 9, 2014
Revised: September 11, 2014

   dx.doi.org/10.1021/sc500436m | ACS Sustainable Chem. Eng. XXXX, XXX, XXX−XXX

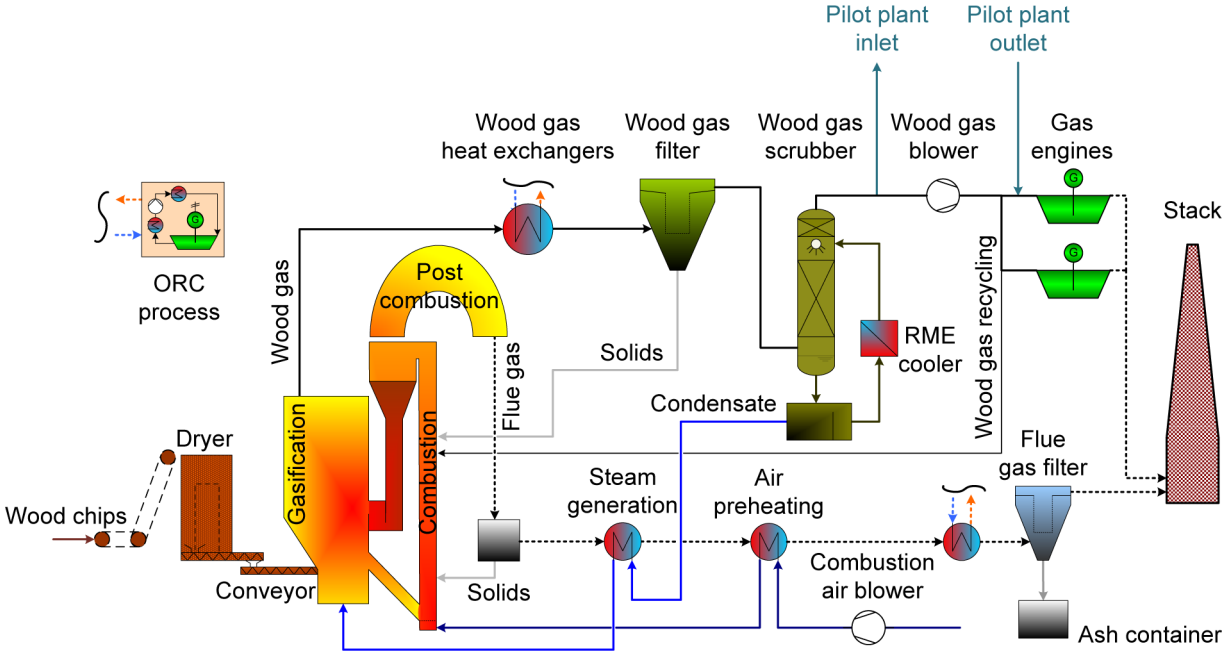

Figure 1. Flowchart of the biomass gasification plant Oberwart including the sampling point of wood gas of the investigated pilot plant. Reprinted with permission from ref 12. Copyright (2013) Nicolas Diaz.

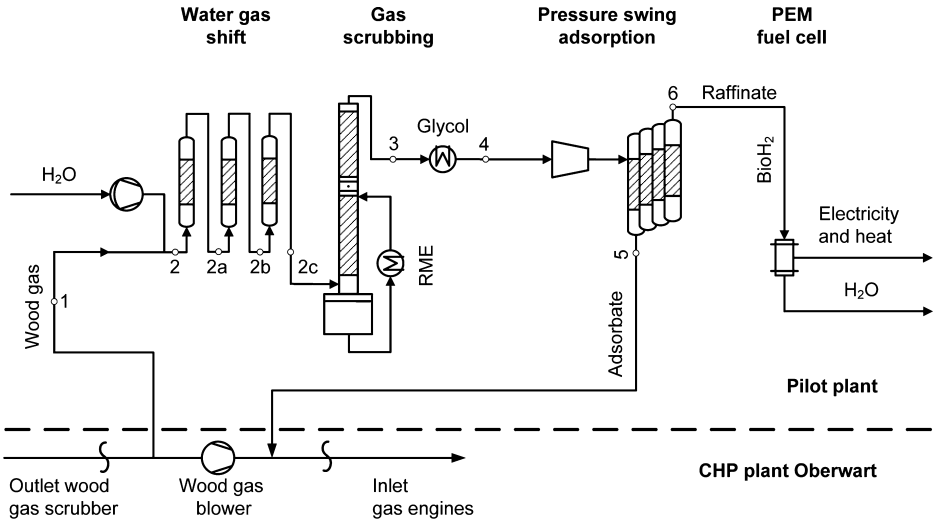

Figure 2. Flowchart of the investigated pilot plant for $BioH_2$ production, including the applied sampling points (1–6) for chemical analysis.

already removed in a baghouse filter, and the majority of the tar was already separated in a gas scrubber operated with rapeseed oil methyl ester (RME). The wood gas extraction point and the point of recycling are plotted in Figure 1 (pilot plant inlet and outlet).

The applied unit operations for wood gas conditioning involved: (I) carbon monoxide conversion via sulfur tolerant catalysis of the water–gas shift (WGS) reaction, (II) gas cleaning in a wet scrubber operated with RME, (III) pressure swing adsorption (PSA) for hydrogen purification, and (IV) application of $BioH_2$ in a proton exchange membrane (PEM) fuel cell.

(I) Catalysis of the WGS reaction (eq 1) is a state of the art technology. A two-stage system with different catalysts is industrially applied in order to produce additional hydrogen by the conversion of carbon monoxide with steam.[15]

$$CO + H_2O \rightleftharpoons H_2 + CO_2 \quad \Delta H_R^0 = -41.1 \frac{kJ}{mol} \tag{1}$$

(II) Wood gas contains traces of ammonia, sulfur components, benzene, toluene, ethylbenzene, and xylene (BTEX), as well as condensable organic compounds (tar). A highly effective approach toward the removal of tar is the absorption in organic solvents (e.g., biodiesel or RME). In parallel, condensing water enables a removal of water-soluble impurities like ammonia and hydrogen sulfide.[16]

(III) The PSA process is based on the physical binding of gas molecules to a solid adsorbent material. The interaction between the gas and the adsorbent depends mainly on the gas component, its partial pressure, the type of adsorbent, and temperature. Hydrogen is a highly volatile compound with a low polarity, and its adsorption capacity on activated carbon is very low.[17]

dx.doi.org/10.1021/sc500436m | ACS Sustainable Chem. Eng. XXXX, XXX, XXX–XXX

(IV) As a demonstration of the high quality of the product, its use in a PEM fuel cell was chosen. The principles of a PEM fuel cell are reviewed in ref 18. In order to meet the requirements of this fuel cell type, the presence of certain wood gas components in the generated $BioH_2$ had to be avoided. In the following, the influence of the relevant wood gas components on a PEM fuel cell are reviewed.

CO is adsorbed on the active surface of the platinum catalyst of a PEM fuel cell and reduces the available area for H_2 oxidation. Concentrations as low as 0.5 to 4.5 vol ppm have been reported to cause performance losses due to a voltage drop that is directly proportional to the CO concentration.[19] CO_2 causes a more pronounced performance loss than inert components like N_2. The reason seems to be the formation of CO, either through the reverse WGS reaction or an electrochemical reduction reaction. Severe performance loss has been reported for CO_2 concentrations of about 20 vol % and higher.[20] H_2S is also adsorbed on the catalyst surface and reduces the area for H_2 oxidation. This mechanism was even observed at concentrations as low as 0.25 vol ppm. In contrast to CO poisoning, the adsorption of H_2S seems to be irreversible.[20] Also carbonyl sulfide (COS) is reported to reduce the active surface of the catalyst.[21] NH_3 is oxidized to NH_4^+ ions, which reduces the proton concentration at the catalyst layer and leads to a reduction of the performance of the anode. After long exposure times, NH_4^+ ions migrate into the proton exchange membrane, resulting in a conductivity loss. These effects have already been observed at ammonia concentrations as low as 1 vol ppm.[20] Inert components like N_2 reduce the partial pressure of H_2, which leads to a potential loss according to the Nernst equation. Apart from this effect, even a high CH_4 concentration shows no negative effects on the performance of a PEM fuel.[22] The O_2 content in the $BioH_2$ needs to be as low as possible in order to avoid the direct formation of water at the anode.[20]

EXPERIMENTAL SECTION

The studied process chain shown in Figure 2 is the third configuration for $BioH_2$ production, which has been tested experimentally at Oberwart. A series of test campaigns, which included a membrane separation unit, were carried out in 2013, and its results have been already published.[12,23]

The current configuration can be seen as a polygeneration concept, aiming at the simultaneous production of H_2, electricity, and district heat. Electricity production can be achieved via combustion of the adsorbate fraction of the PSA unit. The complexity and costs of investment, as well as the operating expense should be kept low, with high overall efficiencies and an acceptable H_2 recovery (H_2 rec) calculated according to the molar flow rate of hydrogen at the inlet and at the outlet of the process chain (eq 2). Therefore, a steam reformer for CH_4 and tar reforming was not desired, although it enables an increased hydrogen yield per biomass input.

$$H_2\text{rec} = \frac{\dot{n}_{H_2,\text{out}}}{\dot{n}_{H_2,\text{in}}} \tag{2}$$

Water–Gas Shift Unit. WGS catalysis was realized in three fixed bed reactors connected in series. A picture of the experimental setup for the catalysis of the WGS reaction is in the Supporting Information. A commercial Fe_2O_3/Cr_2O_3-based catalyst was applied for heterogeneous fixed bed catalysis of the WGS reaction. Prior to the operation of the process chain, the catalyst had been activated according to eq 3 in order to form the catalytically active magnetite (Fe_3O_4). The overall hydrogen demand for this reduction process was negligible (about 1 m_n^3). After the activation of the catalyst, the WGS unit had been commissioned with real wood gas and operated continuously for almost 400 h at an inlet temperature of each reactor of 350 °C. During this conditioning phase, FeS had been formed according to the equilibrium reaction in eq 4. This sulfiding reaction is reversible, and H_2S will be released if the reaction temperature is increased or if the partial pressure of H_2S in the feed is decreased. With respect to the equilibrium constant of the reaction, it can be considered that the loading of FeS is increased by a factor of 6.5 if the temperature is decreased from 400 to 300 °C. FeS is reported to exhibit an activity reduced by 50% compared to magnetite.[15,24]

$$3Fe_2O_3 + H_2 \rightleftharpoons 2Fe_3O_4 + H_2O \quad \Delta H_R^0 = -16.3\frac{\text{kJ}}{\text{mol}} \tag{3}$$

$$Fe_3O_4 + 3H_2S + H_2 \rightleftharpoons 3FeS + 4H_2O \quad \Delta H_R^0 = -75.0\frac{\text{kJ}}{\text{mol}} \tag{4}$$

Steam was added to the wood gas in order to enhance the shift reaction and to prevent carbon formation on the surface of the catalyst.[25] The wood gas flow rate over the WGS unit was set with the rotational speed of the compressor of the PSA unit. The gas at the inlet of each reactor was electrically heated, and the temperature was monitored every 10 cm along the fixed bed. A temperature profile along the three reactors was set, attempting to optimize the overall CO conversion rate. Equilibrium calculations of the WGS reaction have been accomplished using the software HSC. Table 1 summarizes the operating conditions of the WGS unit. In the following, ± denotes the standard deviation of the measured values. The CO conversion rate (X_{CO}) defined in eq 5 was used to describe the performance of the WGS unit. The gas hourly space velocity (GHSV) was calculated using eq 6.

Table 1. Operating Conditions of the WGS Unit

	value	unit
wood gas in	0.56 ± 0.02	$(m_{n\,db}^3)/h$
water addition	0.55 ± 0.02	(kg)/h
T_{in} reactor 1	403 ± 5	°C
T_{in} reactor 2	358 ± 3	°C
T_{in} reactor 3	309 ± 3	°C
pressure	76 ± 7	mbarg
$GHSV_{wet}$	170 ± 5	h^{-1}
$(H_2O)/(CO)$ molar ratio	5 ± 0.2	–
$(H_2O)/C$ molar ratio	2 ± 0.1	–

$$X_{CO} = \frac{\dot{n}_{CO,\text{in}} - \dot{n}_{CO,\text{out}}}{\dot{n}_{CO,\text{in}}} \tag{5}$$

$$\text{GHSV} = \frac{\dot{V}_{\text{gas}}}{V_{\text{catalyst}}} \tag{6}$$

Scrubber Unit. The water–gas-shifted gas subsequently entered a wet scrubbing unit in order to be cleaned and dried for PSA operation. A pipe with a length of 22 m was installed to connect the outlet of the WGS unit with the inlet of the scrubber unit. The heat losses over this length resulted in a rather low inlet temperature of the scrubber. A counter current flow of wood gas and organic solvent (RME) was realized over a structured packed column. The RME was cooled with a plate heat exchanger provided with cold ethylene glycol from an external chiller. In order to ensure complete gas drying, a gas washing bottle filled with ethylene glycol cooled to 0 °C was implemented afterward. The operating conditions of the scrubbing unit are listed in Table 2. A detailed description of the scrubber unit is provided in ref 12. Tar components represent a potential risk for the WGS catalyst as they might serve as precursors for the formation of coke.[26] However, the scrubber was placed downstream of the WGS unit in order to avoid an additional energy intensive cycle of condensation and evaporation.

dx.doi.org/10.1021/sc500436m | ACS Sustainable Chem. Eng. XXXX, XXX, XXX–XXX

Table 2. Operating Conditions of the Scrubber Unit

	solvent	value	unit
T_{in} gas	RME	48.3 ± 2.4	°C
T_{out} gas	RME	5.1 ± 0.2	°C
pressure	RME	58.5 ± 5.8	mbarg
circulation rate	RME	700	L/h
fresh addition	RME	0.5	L/h
T_{out} gas	glycol	0	°C

Pressure Swing Adsorption Unit. The cleaned gas was further processed in a PSA unit for H_2 purification. A picture of this setup is in the Supporting Information. The unit consisted of four vessels with a capacity of 4.72 L each. Every reactor was filled with 2.5 kg of activated carbon (Norit, RB2) as the adsorption agent. The volumetric flow rates of PSA feed and raffinate ($BioH_2$) were quantified with diaphragm gas meters enabling an accurate mass balance of the PSA unit. The adsorption pressure was built up with a gas compressor and the desired desorption pressure was achieved using a diaphragm vacuum pump. The PSA unit was operated in a cyclic sequence, which is described in detail in ref . Raffinate was generated during the adsorption step of one vessel carried out over a variable time frame (adsorption time). During the pressure equalization step, the product of one loaded vessel was used to partly repressurize a currently regenerated adsorber. The equalization pressure (in bara) is defined as the value to which the pressure drops in the gas dispensing vessel. The applied adsorption time and equalization pressure for the long-term experiment were estimated in a previous parameter study. During this study, the adsorption time per column was varied between 400 and 800 s, and the equalization pressure was set to the values 4.0 and 4.5 bara. Table 3 summarizes the basic operating conditions of the PSA unit, which were chosen during the continuous long-term operation.

Table 3. Operating Conditions of the PSA Unit

	value	unit
adsorption pressure	6.5	bara
desorption pressure	0.1	bara
purge/feed time ratio	5×10^{-3}	–
feed flow rate	0.7 ± 0.04	$(m^3_{n\ db})$/h
feed pressure	1000 ± 17	mbara
adsorption time per column	650	s
equalization pressure	4.5	bara

Fuel Cell Unit. A proton exchange membrane (PEM) fuel cell from AXANE was operated with the generated $BioH_2$ to demonstrate its quality. A picture of the employed fuel cell is in the Supporting Information. As a benchmark, the PEM fuel cell was also operated with Alphagaz 1 (H_2 purity > 99.999 vol %). Key data of this PEM fuel cell are listed in Table 4 provided by ref 27.

Chemical Analysis and Mass Balance. This section describes the adopted methods of chemical analysis. Extensive analyses of the main gas components, sulfur components, tar, water, BTEX, and ammonia were carried out. The selected sampling points (S.pt.) of the process chain are illustrated in Figure 2. A matrix of the analyzed components at the available sampling points is provided in the Supporting Information. Prior to gas chromatography (GC) analysis, the water-containing sampling streams were dried over two gas washing bottles filled with ethylene glycol, which were connected in series. The flasks were placed in a temperature-controlled cooling box at −3 °C. A flask filled with glass wool was subsequently removing aerosols from the stream. The sampling flow rate was adjusted with a needle valve upstream to a vacuum pump. A gas meter from Kromschröder (BKG2.5T) was used to quantify the volumetric flow rate of the dry sampling gas at ambient pressure. A corresponding increase in weight of the ethylene glycol filled flasks enabled a parallel estimation of the water content. A figure of the sampling line is in the Supporting Information.

Table 4. Key Data of the PEM fuel cell Unit[a]

	value	unit
nominal voltage DC	48	V
nominal voltage AC	230	V
minimum $power_{el}$	500	W
maximum $power_{el}$	2500	W
H_2 quality (ISO 14687)	99.99	vol %
H_2 operating pressure	250 ± 30	mbarg
H_2 consumption at max. power	35.1	L_n/min
H_2 peak consumption	60	L_n/min

[a]Based on ref 27.

The main gas components (CO_2, N_2, CO, O_2, CH_4, C_2H_6, C_2H_4, and C_2H_2) were separated in a combination of two different columns (7′ HayeSep N, 60/80 1/8″ SF and 9′ molecular sieve 13× 45/60, 1/8″ SF) in a GC (Clarus 500) from PerkinElmer. A thermal conductivity detector (TCD) was used for quantification. The sulfur components (H_2S, COS, C_4H_4S, CH_3CH_2SH, and CH_3SH) were separated in a different column (Rt-XL sulfur 1 m.x 0.95 mm OD) and quantified by a flame photometric detector (FPD).

Tar sampling is also illustrated in the Supporting Information. A combination of two cooling boxes was applied. Scrubbing bottles filled with 50 or 100 mL of toluene were applied to dissolve tar components. Three gas washing bottles were placed in an ice bath at 0 °C, and two additional impingers were placed in a temperature-controlled cooling box at −8 °C. For each tar analysis, a sampling stream of 2 L_n/min was taken over a period of 8 h. For detection of the tar components, a GC from PerkinElmer (XL GC) coupled with a mass spectrometer from PerkinElmer (Turbo Mass MS) was used. A detailed description of the applied method for tar analysis can be found in ref 28.

BTEX values were measured by gas chromatography-mass spectrometry (GC-MS, Shimadzu QP2010 Plus) at Vienna University of Technology. Six samples of each relevant point of the process were taken by means of gas sampling bags. For the quantification of NH_3, an absorption method was used. A sample of 1 L_n/min was extracted from the process for 3 h and passed through three gas washing bottles connected in series in a cooling bath at 0 °C. The bottles were filled with 0.05 M H_2SO_4, which solves NH_3 in the form of NH_4^+ ions. NH_4^+ ions were quantified by ion chromatography (Dionex ICS 5000).

It could be considered that the wood gas fed into the pilot plant was saturated with water corresponding to the operation temperature and pressure of the CHP plant scrubber.[16] The water addition upstream of the catalyzed WGS reaction was quantified gravimetrically and monitored with a variable area flow meter. Additionally, the flow rate of condensate formed in the scrubber was quantified volumetrically. The H_2 content in the dry gas was determined via mass balance. Volumetric flow rates of the dry PSA feed and the raffinate were quantified by diaphragm gas meters. The adsorbate flow rate and composition were calculated via mass balance. The flow rate of the wood gas at the inlet of the WGS unit was calculated via mass balance based on the feed flow rate of the PSA and the change of the gas composition according to the WGS reaction.

RESULTS AND DISCUSSION

During the presented long-term experiment, the CHP plant Oberwart was constantly generating an average of 2100 $m^3_{n\ db}$/h of wood gas, of which 350 $m^3_{n\ db}$/h were recycled back into the combustion zone of the DFB reactor. The outlet temperature of the CHP plant scrubber was 35 ± 6 °C. Assuming a relative humidity of 100% at the outlet of this scrubber, a humidity of approximately 5 mol $\%_{wb}$ could be calculated in the feed gas of the experimental setup.[16]

The pilot plant for H_2 production was successfully operated continuously for almost 250 h. This section gives an overview of the performance of each operation unit as well as the results

dx.doi.org/10.1021/sc500436m | ACS Sustainable Chem. Eng. XXXX, XXX, XXX−XXX

of the detailed chemical analysis of the entire process chain. The results of the chemical analysis are presented with respect to the analyzed substance class (main gas components, sulfur components, BTEX components, tar components, and ammonia). Next, the mass balance of the process is presented and visualized in a Sankey diagram. Finally, the issue energy consumption is discussed, and a brief outlook is given.

Water−Gas Shift Unit. The performance of the WGS unit is illustrated in Figure 3, summarizing all three reactors. The

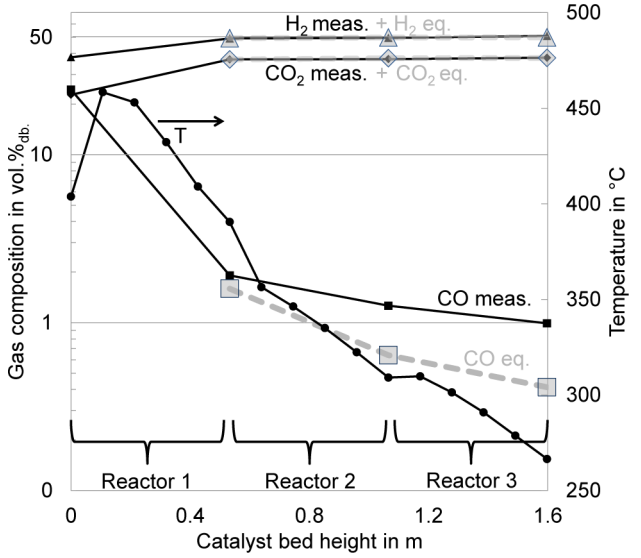

Figure 3. Results of the WGS unit, measured (meas.) and equilibrium (eq) gas composition as well as temperature along the bed height; the sulfidation procedure (eq 4) at the present operating temperature was only completed for reactors 1 and 2 (also see Table 7).

measured gas compositions are plotted on a logarithmic scale and can be compared with the WGS equilibrium at the corresponding outlet temperature of each reactor. Within the first 10 cm of the catalyst bed in the first reactor, the temperature increased by about 60 °C due to the exothermic WGS reaction. The temperature profile demonstrates that the main share of CO was converted within this section of the catalyst bed. Subsequently, the temperature along the bed height decreased due to heat losses. The inlet temperatures of reactors 2 and 3 were steadily lowered in order to harness lower equilibrium CO contents.

At the outlet of the WGS unit, the CO content could be reduced to about 1 vol $\%_{db}$ (also see Table 6), representing a CO conversion rate of 95% and a H_2 recovery of 160% within this unit. The dry volumetric flow rate was increased from 0.56 $m^3_{n\ db}/h$ to 0.70 $m^3_{n\ db}/h$, while the H_2O content was lowered from 56 to 45 mol $\%_{wb}$. Low GHSV, low sulfur loads in the feed gas (see Table 7), and the approach of temperature optimization enabled high overall conversion rates.[15] However, especially in reactors 2 and 3 a complete equilibration of the WGS reaction could not be reached. In order to further enhance the CO conversion in these reactors, the temperature should have been set higher. This is demonstrated by an increasing deviation of the equilibrium CO content and the measured CO content. By means of this, the amount of catalyst could have been reduced significantly maintaining the same CO conversion rate. Industrially applied FeO_3/Cr_2O_3-based catalysts are operated at GHSV of 400−1200 h^{-1}.[2]

Scrubber Unit. The scrubber unit was capable of cooling the shifted gas to 0 °C. Hence, it could be assumed that only a negligible amount of H_2O was present at the inlet of the PSA unit. A condensate flow rate of 0.32 L/h was generated in the scrubber, which corresponded to the overall water balance of the process chain. The performance of the scrubber in terms of tar separation and removal of other undesired gas components is shown in Tables 7−10.

Pressure Swing Adsorption Unit. A parameter study of the PSA unit was carried out previous to the long-term experiment. During the study, a steady state operation of the upstream equipment was maintained. The operation parameters adsorption time and equalization pressure were varied, revealing a trade-off between the purity of the product and the H_2 recovery. At a fixed equalization pressure (4.5 bara), the effect of a variation in adsorption time on the content of the impurities is shown in Figure 4. Increasing amounts of contaminants were analyzed at longer adsorption times. Similar results were achieved at an equalization pressure of 4.0 bara.

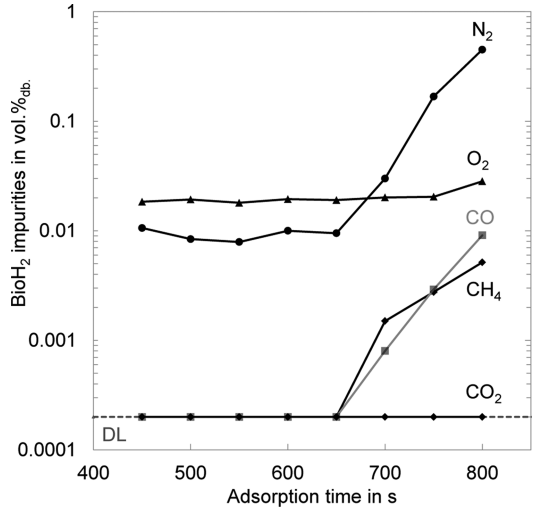

Figure 4. Results of PSA parameter study. $BioH_2$ impurities over adsorption time at an equalization pressure of 4.5 bara; detection limit (DL) = 2 vol ppm.

The influence of varying pressure equalization as well as adsorption time on the H_2 recovery is shown in Figure 5. As shown, the H_2 recovery was improved at lower equalization pressures of the PSA unit.

The aim of this study was to optimize the H_2 recovery provided that the components CO, CO_2, and CH_4 were reduced below the detection limit (BDL, 2 vol ppm_{db}). As a result, the parameters in Table 3 (adsorption time of 650 s and equalization pressure of 4.5 bara) were chosen for the reported steady state operation during the 250 h of continuous experimentation.

Under these fixed conditions, a H_2 purity of 99.97 vol $\%_{db}$ as well as a H_2 recovery of 80.0% were reached. These results are within the range of similar reported PSA systems obtaining H_2 purities up to 99.99 vol $\%_{db}$ and H_2 recoveries between 70% and 85%.[29−33] The volumetric feed flow rate of 0.70 $m^3_{n\ db}/h$ was split into an adsorbate fraction of 0.42 $m^3_{n\ db}/h$ and a raffinate fraction ($BioH_2$) of 0.28 $m^3_{n\ db}/h$. As shown in Table 6, the only detected impurities in the PSA raffinate were O_2 with 0.02 vol $\%_{db}$ and N_2 with 0.01 vol $\%_{db}$.

dx.doi.org/10.1021/sc500436m | ACS Sustainable Chem. Eng. XXXX, XXX, XXX−XXX

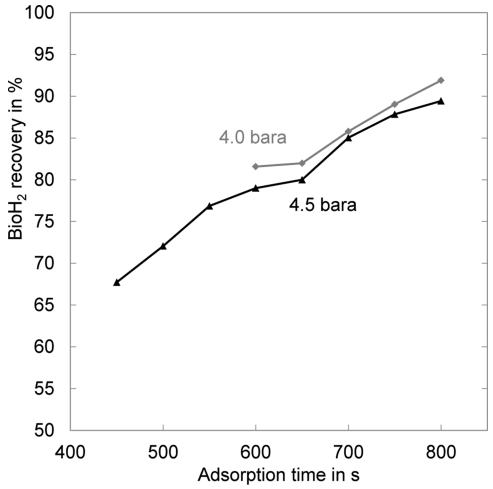

Figure 5. Results of PSA parameter study. $BioH_2$ recovery over adsorption time at an equalization pressure of 4.0 and 4.5 bara.

Fuel Cell Unit. To demonstrate the high purity of the PSA raffinate, the generated $BioH_2$ was fed into a PEM fuel cell (Mobixane from AXANE). The unit was operated flawlessly for over 3 h. The comparison between its operation with the produced $BioH_2$ and Alphagaz 1 H_2 is shown in Table 5.

Table 5. Comparison of PEM fuel Cell Performance with $BioH_2$ and Alphagaz 1

	$BioH_2$	Alphagaz	unit
purity	≥99.97	≥99.999	vol %
$\dot{V}_{H_2}$	0.28 ± 0.01	0.28 ± 0.01	m^3_n/h
p_{Feed}	1268 ± 27	1245 ± 24	mbara
$T_{Fuel\ cell}$	40.5 ± 1.5	36.8 ± 0.9	°C
η_{gross}	53.9 ± 1.0	54.2 ± 1.0	$\%_{LHV\ base}$

It could be demonstrated that there was no significant difference in the fuel cell performance comparing the operation with $BioH_2$ and the operation with Alphagaz 1 in the investigated period. This can be distinguished between the gross electrical efficiency and net electrical efficiency of the fuel cell. In Table 5, the gross electrical efficiencies are presented. The inverter and the peripherals of the fuel cell cause a decrease in its electrical efficiency and account for the net electrical efficiency. A gross electrical efficiency of about 54% was obtained, which is in good accordance to ref 21. The obtained value for the net electrical efficiency was not representative as the unit was operated below its nominal power range. The issue of electrical efficiencies and the setup of this fuel cell are described in detail in refs 12 and 34.

Chemical Analysis and Mass Balance. In this chapter, the evolution of the dry gas composition along the process chain is presented. The results have to be regarded in combination with the corresponding sampling points (S.pt.) illustrated in Figure 2. All results are measured gas compositions, except for the mean adsorbate composition, which was calculated via mass balance (the feed flow rate and the composition of the adsorbate vary strongly as a function of the cyclic PSA operation). Table 6 depicts the evolution of the main gas components on a dry base, detected with the TCD detector of the GC.

In Table 6, the given CO concentrations over the WGS unit represent a CO conversion rate of about 90.5% at the outlet of

Table 6. Results of Analysis of Main Gas Components[a]

S.pt.	CO_2 (vol $\%_{db}$)	C_2H_4 (vol $\%_{db}$)	C_2H_6 (vol $\%_{db}$)
1	22.7 ± 0.8	2.3 ± 0.3	0.17 ± 0.03
2a	36.9 ± 0.8	1.8 ± 0.1	0.17 ± 0.02
2b	37.0 ± 0.8	1.8 ± 0.1	0.17 ± 0.03
2c	37.1 ± 0.9	1.9 ± 0.2	0.18 ± 0.02
4	36.9 ± 0.2	1.6 ± 0.3	0.14 ± 0.03
5	61.4	2.6	0.23
6	BDL	BDL	BDL
S.pt.	C_2H_2 (vol $\%_{db}$)	O_2 (vol $\%_{db}$)	N_2 (vol $\%_{db}$)
1	0.15 ± 0.02	0.1 ± 0.02	2.3 ± 0.4
2a	0.001 ± 0.001	0.06 ± 0.01	1.8 ± 0.1
2b	BDL	0.08 ± 0.04	2 ± 0.1
2c	BDL	0.07 ± 0.06	1.9 ± 0.3
4	BDL	0.03 ± 0.01	1.5 ± 0.1
5	BDL	0.03	2.6
6	BDL	0.02 ± 0.0003	0.01 ± 0.004
S.pt.	CH_4 (vol $\%_{db}$)	CO (vol $\%_{db}$)	H_2 (vol $\%_{db}$)
1	10.0 ± 0.3	24 ± 1	38.0 ± 1.2
2a	8.2 ± 0.1	1.9 ± 0.3	49.2 ± 0.9
2b	8.1 ± 0.2	1.3 ± 0.2	49.5 ± 0.9
2c	8.2 ± 0.2	1.0 ± 0.1	49.6 ± 0.9
4	8.0 ± 0.2	0.98 ± 0.04	50.9 ± 0.4
5	13.3	1.63	18.2
6	BDL	BDL	99.97 ± 0.004

[a]Sampling points (S.pt.) are illustrated in Figure 2; BDL = below detection limit, DL = 2 vol ppm_{db}; adsorbate composition (5) was calculated via mass balance.

the first reactor ($GHSV_{wb}$ 510 h^{-1}) and a CO conversion rate of about 93.5% at the outlet of the second reactor ($GHSV_{wb}$ 255 h^{-1}). At the outlet of the last reactor ($GHSV_{wb}$ 170 h^{-1}), an overall CO conversion rate of about 95% was reached. The H_2 content was increased from 38 vol $\%_{db}$ to about 50 vol $\%_{db}$. The simultaneous increase in the dry gas flow rate by 25% led to a general dilution effect. C_2H_2 was totally hydrogenated to C_2H_4 and could not be detected at the outlet of the WGS unit. C_2H_4 was assumed to be partly hydrogenated to C_2H_6. The overall mass balance of the C_2H_y components was approaching 98%. The slightly higher content of H_2 in the PSA feed (4) compared to the outlet of the WGS unit (2c) could be explained by the low solubility of hydrogen in water as well as by the removal of a series of gas components in the scrubber unit (e.g., benzene and ammonia). It is also shown that O_2 and N_2 were the only detectable impurities that were fed into the fuel cell. O_2 is reported to be tolerated up to 500 vol ppm, and N_2 has only dilution effects on the PEM fuel cell.[20]

The evolution of the sulfur components along the process is provided in Table 7.

Table 7. Results of Analysis of Sulfur Components[a]

S.pt.	H_2S (vol ppm_{db})	COS (vol ppm_{db})	C_4H_4S (vol ppm_{db})
1	59 ± 10	1.0 ± 0.1	7.2 ± 3.1
2a	49 ± 4	BDL	2.0 ± 0.7
2b	50 ± 3	BDL	1.0 ± 0.5
2c	4 ± 1	BDL	1.0 ± 0.6
4	2.5 ± 0.3	BDL	0.3 ± 0.01
5	0.4 ± 0.3	BDL	0.5 ± 0.3
6	BDL	BDL	BDL

[a]DL = 0.3 vol ppm_{db}.

dx.doi.org/10.1021/sc500436m | ACS Sustainable Chem. Eng. XXXX, XXX, XXX−XXX

As proved by constant H_2S concentrations, the catalyst sulfidation was completed in the first two reactors, where the main CO conversion took place. However, only 4 vol ppm_{db} of H_2S was measured after the third reactor, which shows an incomplete sulfidation of this stage during the presented study. Compared to the conditioning of the catalyst (carried out before the test run, 400 h of operation at 350 °C), the last reactor was now operated at a lower temperature level, which provided a favorable condition for an enhanced catalyst sulfidation.[35] The WGS unit was basically designed for higher GHSV than applied during the operation of the process chain. In more recent experiments, the same conversion rate of 95% could be achieved with the completely sulfided catalyst (same concentration of H_2S at the inlet and outlet) at $GHSV_{wb}$ of about 500 h^{-1} and slightly higher operating temperatures.

COS was not detected at the outlet of the WGS unit, which could be explained by the reactions shown in eqs 7 and 8. The decrease in thiophene (C_4H_4S) along the WGS unit is suggested to be due to the reaction of thiophene hydrogenolysis in eq 9.[15] Less C_4H_4S and H_2S could be detected after gas scrubbing. The organic C_4H_4S was assumed to dissolve in the RME, whereas the H_2S dissolved in the condensate. Table 7 also indicates that a fraction of the H_2S present in the feed was captured in the PSA unit. However, previous experiments at the PSA unit showed a complete desorption of H_2S from the activated charcoal at higher sulfur loads in the PSA feed.[12] The rather low sulfur load in the adsorbate was explained by adsorption effects of the used gas sampling bag.

$$H_2 + COS \rightleftharpoons H_2S + CO \quad \Delta H_R^0 = 10.9 \frac{kJ}{mol} \tag{7}$$

$$H_2O + COS \rightleftharpoons H_2S + CO_2 \quad \Delta H_R^0 = -30.3 \frac{kJ}{mol} \tag{8}$$

$$C_4H_4S + 4H_2 \rightleftharpoons C_4H_{10} + H_2S \quad \Delta H_R^0 = -261.2 \frac{kJ}{mol} \tag{9}$$

Analyses of BTEX are shown in Table 8. In the WGS unit, no significant change in the content of benzene, toluene, and xylene could be observed, apart from a dilution effect due to an increased volumetric gas flow rate. The hydrogenation of styrene (Table 9) was assumed to be responsible for the formation of the ethylbenzene as a side reaction in the WGS unit. The scrubber unit removed the majority of the BTEX compounds. Only benzene and toluene could be detected at the inlet of the PSA unit. Analysis of the PSA raffinate and adsorbate suggests a complete adsorption and subsequent desorption of these compounds from the activated carbon.

Table 8. Results of Analysis of Benzene (B), Toluene (T), Ethylbenzene (E), and Xylene (X)[a]

S.pt.	B	T	E	X
1	3296 ± 36	201 ± 5	1.3 ± 0.6	1.1 ± 0.6
2c	2850 ± 54	176 ± 6	33 ± 12	2.2 ± 0.9
4	536 ± 5	17 ± 2	BDL	1.2 ± 0.6
5	641 ± 13	21 ± 1	BDL	BDL
6	BDL	BDL	BDL	BDL

[a]BTEX, in vol ppm_{db}; DL = 1 vol ppm_{db}.

The results of the tar analysis in Table 9 are based on three continuous long-term samples. Therefore, no standard deviations can be given. As a side reaction in the WGS unit, styrene and indene were probably hydrogenated to form ethylbenzene (Table 8) and indane (not analyzed). Furthermore, a hydrogenation of phenylacetylene to ethylbenzene as well as a hydrogenation of acenaphthylene to acenaphthene could be assumed. Besides the frequently observed dilution effect, naphthalene as the predominant tar component was probably not affected in the WGS unit. In the scrubbing unit, all measured tar components except naphthalene could be removed to below the detection limit.

Table 9. Results of Analysis of Tar Components (one continuous sample)[a]

	S.pt.		
tar component	1 ($mg/m^3_{n\ db}$)	2c ($mg/m^3_{n\ db}$)	3 ($mg/m^3_{n\ db}$)
naphthalene	1139	824	2
styrene	247	BDL	BDL
indene	191	9	BDL
phenylacetylene	25	BDL	BDL
mesitylene	BDL	4	BDL
benzofuran	2	BDL	BDL
1-benzothiophene	2	BDL	BDL
2-methylnaphthalene	5	4	BDL
1-methylnaphthalene	3	2	BDL
biphenyl	1	BDL	BDL
acenaphthylene	13	BDL	BDL
acenaphthene	2	7	BDL
anthracene	2	4	BDL
flouranthene	1	3	BDL
pyrene	1	3	BDL

[a]DL = 1 $mg/m^3_{n\ db}$.

The results of the NH_3 analysis in Table 10 are also based on one continuous sample per sampling point. Therefore, no standard deviations can be given. Apart from the dilution effect in the WGS unit, no influence of the catalyst on the NH_3 was observed. In the scrubbing unit, the amount of NH_3 was reduced below the detection limit. Hence, there was no NH_3 present at the inlet of the PSA unit.

Table 10. Results of Analysis of NH_3 (one continuous sample)[a]

S.pt.	NH_3 (vol ppm_{db})
1	954
2c	740
3	1
4	BDL

[a]DL = 1 vol ppm_{db}.

Summing up, the aim of this polygeneration approach was to minimize its complexity at acceptable H_2 recoveries. The process used one single compression step and worked flawlessly for 250 h. The obtained flow rates and water contents over the process chain are summarized in Table 11. The global mass balance of the established process is also illustrated by means of the Sankey diagram in Figure 6. The width of the arrows is shown proportionally to the molar flow of each component.

The diagram shows that more H_2 could be separated in the PSA unit than H_2 was present in the wood gas feed. The overall hydrogen recovery of 128% was enabled by the production of additional H_2 in the WGS unit (recoveries of the single process

dx.doi.org/10.1021/sc500436m | ACS Sustainable Chem. Eng. XXXX, XXX, XXX−XXX

Table 11. Mass balance and H_2O Content over the Process Chain[a]

S.pt.	description	Flow rate ($m^3_{n\ wb}$)/h	H_2O (vol $\%_{wb}$)
1	raw gas	0.60	5.21
2	WGS in	1.28	55.82
2c	WGS out	1.28	45.46
3	RME out	0.71	0.84
4	PSA in	0.70	0
5	adsorbate	0.28	0
6	$BioH_2$	0.42	0

[a]Water considered as an ideal gas at standard conditions.

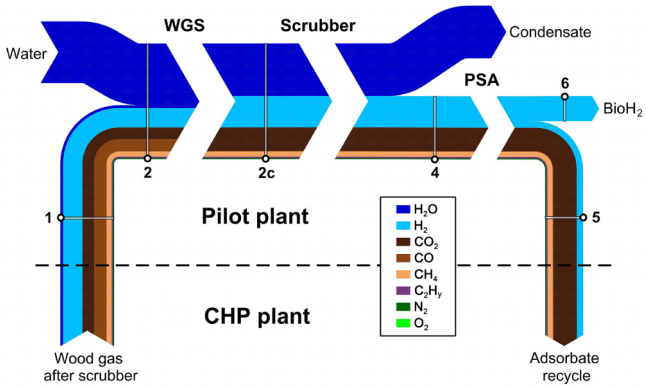

Figure 6. Sankey diagram of the process chain. The width of the arrows is shown proportionally to the molar flow of each component, including sampling points of chemical analysis.

steps: 160% in the WGS unit, 100% in the gas scrubber, and 80% in PSA unit).

A total of 0.56 $m^3_{n\ db}$/h of dry wood gas was extracted after the scrubber of the CHP plant Oberwart. Catalysis of the WGS reaction caused an increase in the dry volumetric flow rate to 0.70 $m^3_{n\ db}$/h, decreasing the CO content from about 24 to 1 vol $\%_{db}$. In the PSA unit, the feed was split into 0.42 $m^3_{n\ db}$/h of adsorbate and 0.28 $m^3_{n\ db}$/h of raffinate. The only detectable impurities in the PSA raffinate were O_2 (0.02 vol $\%_{db}$) and N_2 (0.01 vol $\%_{db}$). This gas composition enabled the operation of a PEM fuel cell.

Within this working group, a master thesis was carried out to evaluate the presented process chain in terms of energy consumption.[36] It was distinguished between the electricity demand for pumps and compressors, the heating demand, and the cooling demand. A specific energy demand of 0.57 (kW h_{el})/(m^3_n $BioH_2$), 1.71 (kW h_{cool})/(m^3_n $BioH_2$), and 2.12 (kW h_{heat})/(m^3_n $BioH_2$) was calculated by means of the process simulation software IPSEpro (LHV of H_2: 3 kWh/m^3_n. In order to reduce the heat demand for steam production, wood gas for $BioH_2$ production should be extracted upstream of the scrubber of the CHP plant. A water content of already 35 mol $\%_{wb}$ can be estimated at this point of the process.[14] In this case, the catalyst of the WGS unit would have to face a considerably higher load of impurities. Future experimental work will cover the long-term stability of the catalyst in combination with this tar-rich wood gas. Apart from this, an adsorption tube will be installed in the feed of the fuel cell in order to reduce the detection limit of impurities in the $BioH_2$.

A positive overall assessment will provide the basis for an upscale of the process to a capacity of about 50 $m^3_{n\ db}$/h $BioH_2$.

■ ASSOCIATED CONTENT

Supporting Information

Pictures of the CHP plant Oberwart, installed WGS unit, PSA unit, and PEM fuel cell. Matrix of the analyzed components and the available sampling points, as well as a flowchart of the sampling line for chemical analysis. This material is available free of charge via the Internet at http://pubs.acs.org.

■ AUTHOR INFORMATION

Corresponding Authors

*E-mail: silvester.fail@gmail.com (S.F.).
*E-mail: nicolas.diaz@gmx.at (N.D.).

Notes

The authors declare no competing financial interest.

■ ACKNOWLEDGMENTS

The authors thank the project partners: Energie Burgenland, Air Liquide, Binder Industrieanlagenbau and CTS. The company Clariant is gratefully acknowledged for providing the WGS catalyst. Especially, the CHP plant Oberwart is thanked for providing a unique working environment and a stable supply of wood gas. The long-term conditioning of the WGS catalyst could only be achieved with the help of Matthias Binder. Christian Jordan is thanked for his commitment related to BTEX analysis. Nicolas Diaz received financial support from Conicyt-Becas Chile. Several research projects collaborated to realize the presented process chain: "Polygeneration 2" (Bioenergy2020+), "Green H_2" (FFG), and "Simple SNG" (FFG). Bioenergy2020+ is funded within the Austrian COMET program managed by the Austrian Research Promotion Agency (FFG). The financial support of the funding association FFG and the Austrian Climate and Energy Fund is gratefully acknowledged.

■ NOMENCLATURE

Abbreviations and Acronyms

a: year (anno)
BDL: below detection limit
$BioH_2$: biohydrogen, hydrogen produced by or out of biomass
BTEX: benzene, toluene, ethylbenzene, xylene
CHP: combined heat and power
C_xH_y: hydrocarbons
DFB: dual fluidized bed
DL: detection limit
FPD: flame photometric detector
GC: gas chromatography
GHSV: gas hourly space velocity
LHV: lower heating value
L: liter
mol: molar
ORC: organic rankine cycle
PEM: proton exchange membrane
PSA: pressure swing adsorption
RME: rapeseed oil methyl ester
S.pt: sampling point
TCD: thermal conductivity detector
t: ton
vol: volumetric
WGS: water−gas shift

Indices

cool: cooling

dx.doi.org/10.1021/sc500436m | ACS Sustainable Chem. Eng. XXXX, XXX, XXX−XXX

db: dry base
el: electric
eq: equilibrium
heat: heating
in: inlet
meas: measured
n: standard conditions (0 °C and atmospheric pressure)
out: outlet
rec: recovery
wb: wet base

Symbols

ΔH_R^0: Standard enthalpy of reaction in (kJ)/(mol) (at 0 °C and 1 bar)
$\eta_{\text{el gross}}$: Gross electrical efficiency, dimensionless
$\dot{n}$: molar flow rate in (mol)/h
$\dot{V}$: Volumetric flow rate in $(m_n^3)/h$
X_{CO}: CO conversion rate, dimensionless

REFERENCES

(1) *Hydrogen Production and Distribution*; Energy Technology Essentials; International Energy Agency: Paris, 2007.
(2) Liu, K.; Song, C.; Subramani, V. *Hydrogen and Syngas Production and Purification Technologies*; Wiley, NewYork, 2010; pp 14−17, 313.
(3) Dunn, S. Hydrogen futures: Toward a sustainable energy system. *Int. J. Hydrogen Energy* **2002**, *27*, 235−264.
(4) Hefner, R. A. The age of energy gases. *Int. J. Hydrogen Energy* **2002**, *27*, 1−9.
(5) Chaubey, R.; Sahu, S.; James, O. O.; Maity, S. A review on development of industrial processes and emerging techniques for production of hydrogen from renewable and sustainable sources. *Renewable Sustainable Energy Rev.* **2013**, *23*, 443−462.
(6) Gahleitner, G. Hydrogen from renewable electricity: An international review of power-to-gas pilot plants for stationary applications. *Int. J. Hydrogen Energy* **2013**, *38*, 2039−2061.
(7) Abbasi, T.; Abbasi, S. Renewable hydrogen production: Prospects and challenges. *Renewable Sustainable Energy Rev.* **2011**, *15*, 3034−3040.
(8) Tock, L.; Maréchal, F. Co-production of hydrogen and electricity from lignocellulosic biomass: Process design and thermo-economic optimization. *Energy* **2012**, *45*, 339−349.
(9) Moreno, J.; Dufour, J. Life cycle assessment of hydrogen production from biomass gasification. Evaluation of different Spanish feedstocks. *Int. J. Hydrogen Energy* **2013**, *38*, 7616−7622.
(10) Susmozas, A.; Iribarren, D.; Dufour, J. Life-cycle performance of indirect biomass gasification as a green alternative to steam methane reforming for hydrogen production. *Int. J. Hydrogen Energy* **2013**, *38*, 9961−9972.
(11) *Booklet Biomassevergasungskraft Oberwart*; Energie Burgenland: Eisenstadt , Austria2014.
(12) Diaz, N. Hydrogen Separation from Producer Gas Generated by Biomass Steam Gasification. Ph.D. Thesis, Vienna University of Technology, 2013.
(13) Hofbauer, H.; Rauch, R.; Bosch, K.; Koch, R.; Aicherning, C. In *Biomass CHP Plant Güssing, A Success Story*; Bridgwater, A., Ed.; CPL Press: Berks, U.K., 2003; pp 527−536.
(14) Kotik, J. Über den Einsatz von Kraft-Wärme-Kopplungsanlagen auf Basis der Wirbelschicht-Dampfvergasung fester Biomasse am Beispiel des Biomassekraftwerks Oberwart. Ph.D. Thesis, Technische Universität Wien, 2010.
(15) Twigg, M. V. *Catalyst Handbook*, 2nd ed.; Manson Publishing: Singapore, 1989; pp 200−201, 283−288, 302−306, Chapter 6.
(16) Pröll, T.; Siefert, I. G.; Friedl, A.; Hofbauer, H. Removal of NH_3 from biomass gasification producer gas by water condensing in an organic solvent scrubber. *Ind. Eng. Chem. Res.* **2005**, *44*, 1576−1584.
(17) Ruthven, D. M. *Pressure Swing Adsorption*; VCH: Weinheim, 1994; pp 235−238.
(18) *Fuel Cell Handbook*; U.S. Department of Energy: Washington, DC, 2004.
(19) Benesch, R.; Jacksier, T. Hydrogen and Material Quality Issues for PEM Fuel Cells. Vehicle Power and Propulsion, 2005 IEEE Conference, 2005; pp 646−651.
(20) Besancon, B. M.; Hasanov, V.; Imbault-Lastapis, R.; Benesch, R.; Barrio, M.; Mlnvik, M. J. Hydrogen quality from decarbonized fossil fuels to fuel cells. *Int. J. Hydrogen Energy* **2009**, *34*, 2350−2360.
(21) Kurzweil, P. In *Brennstoffzellentechnik*; Fister, M., Ed.; Springer Vieweg: Weinheim, Germany, 2013; pp 87, 98.
(22) Blessing, I.; Gardner, C.; Ternan, M. Separation of hydrogen from a hydrogen/methane mixture using a PEM fuel cell. *Int. J. Hydrogen Energy* **2007**, *32*, 908−914.
(23) Fail, S.; Diaz, N.; Konlechner, D.; Hackel, M.; Sanders, E.; Rauch, R.; Harasek, M.; Bosch, K.; Schwenninger, F.; Zapletal, P.; Schee, Z.; Hofbauer, H. An Experimental Approach for the Production of Pure Hydrogen Based on Wood Gasification, Proceedings of the International Conference for Polygeneration Strategies (ICPS), 2013.
(24) Hla, S. S.; AMorpeth, L.; Sun, Y.; Duffy, G.; Ilyushechkin, A.; Roberts, D.; Edwards, J. A CeO_2-La_2O_3-based Cu catalyst for the processing of coal-derived syngases via high-temperature water gas shift reaction. *Fuel* **2013**, *114*, 178−186.
(25) Shiratori, Y.; Ijichi, T.; Oshima, T.; Sasaki, K. Internal reforming SOFC running on biogas. *Int. J. Hydrogen Energy* **2010**, *35*, 7905−7912.
(26) Bartholomew, C. H. Mechanisms of catalyst deactivation. *Appl. Catal., A* **2001**, *212*, 17 − 60, Catalyst Deactivation.
(27) Moine, S. *Mobixane Operation Manual*; Axane Fuel Cell Systems: Sassenage, France, 2009.
(28) Wolfesberger, U.; Aigner, I.; Hofbauer, H. Tar content and composition in producer gas of fluidized bed gasification of wood-influence of temperature and pressure. *Environ. Prog. Sustainable Energy* **2009**, *28*, 372−379.
(29) Yang, J.; Hana, S.; Chob, C.; Lee, C.-H.; Lee, H. Bulk separation of hydrogen mixtures by a one-column PSA process. *Sep. Purif. Technol.* **1995**, *5*, 239−249.
(30) Ribeiro, A. M.; Grande, C. A.; Lopes, F. V.; Loureiro, J. M.; Rodrigues, A. E. A parametric study of layered bed PSA for hydrogen purification. *Chem. Eng. Sci.* **2008**, *63*, 5258−5273.
(31) Park, J.-H.; Kim, J.-N.; Cho, S.-H. Performance analysis of four-bed H_2 PSA process using layered beds. *AIChE J.* **2000**, *46*, 790−802.
(32) Ahn, S.; You, Y.-W.; Lee, D.-G.; Kimb, K.-H.; Oh, M.; Lee, C.-H. Layered two- and four-bed PSA processes for H_2 recovery from coal gas. *Chem. Eng. Sci.* **2012**, *68*, 413−423.
(33) Lopes, F. V.; Grande, C. A.; Rodrigues, A. E. Activated carbon for hydrogen purification by pressure swing adsorption: Multi-component breakthrough curves and {PSA} performance. *Chem. Eng. Sci.* **2011**, *66*, 303−317.
(34) Kraussler, M. PEM Fuel Cell Operation and Applications Using BioH_2. Master of Science Thesis, Vienna University of Technology, 2014.
(35) Morpeth, L.; Sun, Y.; Hla, S. S.; French, D.; Duffy, G.; Edwards, J. Effect of H_2S on the performance of $La_{0.7}Ce_{0.2}FeO_3$ perovskite catalyst for high temperature water-gas shift reaction. *Int. J. Hydrogen Energy* **2012**, *37*, 1475−1481.
(36) Hinteregger, J. Performance Evaluation of Process Chains for the Production of BioH_2 from Wood Gas. Master of Science Thesis, Vienna University of Technology, 2014.